Analysis and Validation for an Inverter-side Current Controller in LCL Grid-connected Power Systems

Jose M. Sosa, Panfilo R. Martinez-Rodriguez, Gerardo Escobar, Gerardo Vazquez, Andres A. Valdez-Fernandez, and Juan F. Martinez-Garcia

***Abstract*—Transformerless grid-connected inverters offer greater efficiencies when transferring power from renewable energy sources to the electrical grid. If the grid-inverter connection is done with an LCL filter, high attenuation of switching harmonics is achieved while preserving a small-size output filter. However, damping must be included in the controller to assure closed-loop stability. This paper proposes a reference computation methodology for the inverter-side current feedback in a photovoltaic (PV) generation system connected to the grid through an LCL filter. Theoretical analysis of the closed-loop system stability and of the steady-state performance are presented as well as experimental validation of the closed-loop performance. The feedback controller includes active damping and relies on a resonant control structure which improves the ability of dealing with grid harmonic distortion. The controller uses a reduced set of measurements, which requires the inverter-side current and grid voltage only, and assures a power factor close to unity.**

***Index Terms*—LCL filter, transformerless inverter, grid connection, inverter-side current feedback.**

I. Introduction

TRANSFORMERLESS power inverters connected to the grid have acquired a notorious usage among residential and industrial facilities. A noteworthy application that is gaining increasing interest is the connection to the grid of renewable sources such as photovoltaic (PV), wind turbine or hybrid generation systems [1]-[3]. In these applications, the electric energy is delivered by compelling a grid-side current with an almost pure alternating-current (AC) sinusoidal waveform with zero phase-shift with respect to the fundamental component of the grid voltage. However, this latter, which is fixed by the grid, may present harmonic distortion.

Transformerless power inverters are connected to the grid through a passive filter. An inductive filter represents one of the simplest solutions for this connection, which leads to simple filter and controller designs, and practical implementations [4]. Most advanced solutions such as LCL or LLCL filters provide increased mitigation of switching harmonics with smaller components, reduced physical space and reduced costs [5], [6]. However, resonant issues arise, and thus, damping must be added to reduce the risk of undesirable oscillating or possibly destructive behaviors. This leads to a more involved control design, which becomes even more challenging in the case of a reduced number of sensors [7], [8].

In LCL grid-connected power inverters, damping can be added by means of additional passive networks. For example, a series resistor or a shunt RC network can be connected to the LCL filter capacitor to add passive damping [9]. Alternatively, advanced controllers can be designed to provide the necessary damping without power dissipation. This strategy, whose efficiency is remarkably better compared to passive damping, is known as active damping [10].

Several controllers providing active damping to the closed-loop system have been proposed so far. Most of them are based on the feedback of the grid-side or inverter-side currents and the feedback of the voltage or current of the LCL filter capacitor [7], [11]-[15]. Other approaches consider a reduced number of measured states by avoiding the measurement of the voltage or current of the LCL filter capacitor. In particular, two main control design approaches can be distinguished to assure active damping. The first approach relies on the feedback of the inverter-side current [7], [11], [14], while the second relies on the feedback of the grid-side current [12], [16], [17]. In the grid-side current feedback, the damping is added only under certain conditions on the LCL filter parameters and switching frequency. This approach may even present instability issues in the presence of weak grid conditions in [17]. In contrast, the inverter-side current

Manuscript received: November 6, 2018; accepted: September 19, 2019. Date of CrossCheck: September 19, 2019. Date of online publication: February 28, 2020.

This article is distributed under the terms of the Creative Commons Attribution 4.0 International License (http://creativecommons.org/licenses/by/4.0/).

J. M. Sosa (corresponding author) and G. Vazquez are with the Tecnologico Nacional de Mexico / ITS de Irapuato (TecNM / ITESI), Irapuato, GTO 36821, Mexico (e-mail: jmsosa@ieee.org; gerardo.vazquez@itesi.edu.mx).

P. R. Martinez-Rodriguez, A. A. Valdez-Fernandez, and J. F. Martinez-Garcia are with the School of Sciences, Autonomous University of San Luis Potosi (UASLP), San Luis Potosi, SLP 78290, Mexico (e-mail: pamartinez@ieee.org; andres.valdez@ieee.org; jfelipe.martinez@ieee.org).

G. Escobar is with Tecnologico de Monterrey, Monterrey, N.L. 64849, Mexico (e-mail: gescobar@ieee.org).

DOI: 10.35833/MPCE.2018.000505

feedback adds sufficient damping to mitigate the resonant behavior of the LCL filter [7], [15] in a broader range of parameters, switching frequency and grid conditions. However, the computation of the inverter-side current reference following this approach is more elaborated. An interesting alternative has been presented in [14], which uses a reduced-order observer to realize a full state-feedback control, where the inverter-side current is the only available state.

This paper analyzes and experimentally validates an inverter-side current controller for power inverters connected to the grid through an LCL filter. The controller consists of a proportional term over the inverter-side current error, and a harmonic compensation mechanism, which is embodied in a bank of resonant filters tuned at the fundamental and harmonic frequencies and also operating on the inverter-side current error. The proportional term adds the required damping, while the resonant control structure compensates the effect of the grid voltage harmonic distortion to assure a high-quality grid current. This controller guarantees the tracking of the inverter-side current. Hence, it is important to provide an appropriate inverter-side current reference. This reference must be designed to assure that the grid-side current follows a sinusoidal waveform of the grid fundamental frequency component only, in phase with the grid voltage. The key to design such a reference is the use of a scheme that extracts the fundamental component of the grid voltage and its square-phase companion. The analysis shows that the inverter-side current controller guarantees asymptotic stability.

Experimental tests are performed in a three-level inverter prototype for simplicity. However, the controller can be extended to other inverter topologies. The experimental results show that the inverter, with the controller and the proposed current reference computation, supplies active power to the grid with a good performance and enough damped response despite the harmonic distortion in the grid voltage. Moreover, the solution uses a reduced number of sensors. The main contribution of the paper is the design of an inverter-side current controller to guarantee active damping for LCL grid-connected *H*-bridge (HB) based converters along with the corresponding stability analysis. The controller is able to achieve active power injection with guaranteed active damping by using a design method to obtain the references for the inverter-side current and the injected voltage. In addition, the corresponding modifications to these references are also included to deal with the more realistic scenario that considers harmonic distortion in the grid voltage.

II. System Modeling

A general representation of a power inverter connected to the grid through an LCL filter to supply power to the grid is depicted in Fig. 1. The inductors L_1 and L_2 and the capacitor C form the LCL filter between the power inverter and the grid. The grid is represented by a sinusoidal voltage source v_S with fundamental angular frequency ω_S that may contain harmonic distortion.

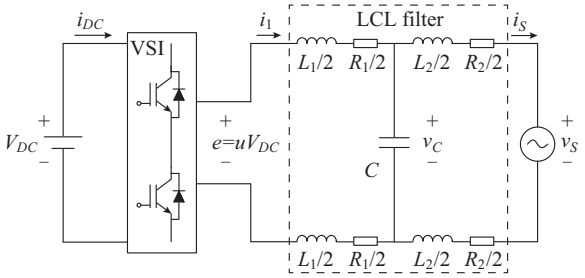

Fig. 1. Power inverter connected to grid through LCL filter.

Let i_1 and i_S denote the currents through L_1 and L_2, respectively, namely the inverter-side and the grid-side currents, and let v_C denote the voltage across C. The model of the system in Fig. 1, is described by the following equations:

$$L_1 \mathrm{d}i_1/\mathrm{d}t = -R_1 i_1 - v_C + e \tag{1}$$

$$L_2 \mathrm{d}i_S/\mathrm{d}t = -R_2 i_S + v_C - v_S \tag{2}$$

$$C \mathrm{d}v_C/\mathrm{d}t = i_1 - i_S \tag{3}$$

where each inductor is represented by an inductance L_i followed by a parasitic resistor R_i, $i = 1, 2$. The main objective is to supply active power to the grid by forcing the grid-side current i_S to have a pure sinusoidal waveform in phase with the fundamental component of the grid voltage v_S. In order to comply with this purpose, the voltage source inverter (VSI) must reconstruct an appropriate voltage signal e, referred to as the inverter voltage and the control objective all along the paper.

In the present work, it is assumed that the switching frequency is high enough, that is, the cutoff frequency of the LCL filter is selected well below the switching frequency f_{sw}. In this way, the ripple in all signals can be neglected, and e can be regarded as a continuous signal. In fact, it can be calculated as $e = uV_{DC}$, as shown in Fig. 1, where $u \in [-1, 1]$ is considered to be continuous and represents the duty ratio of a pulse width modulation (PWM) signal.

The inverter-side current controller, to be described in the next section, can be used without major modifications in several renewable based systems that supply electric energy to the grid. Furthermore, the VSI in Fig. 1 could be any single-phase suitable topology, which is the case of HB-based topologies such as the H5 [18], the HERIC [19], the H6 [20] or the ZVFBR [21] topology. A PV system is taken as an example, where the direct-current (DC) power supply is replaced by an array of PV panels. In this case, the controller must be enhanced with a regulation loop to maintain the DC-link voltage in an average reference value V_{DC} dictated by an additional maximum power point tracking (MPPT) algorithm.

In general, the inductor series parasitic resistors R_1 and R_2 shown in Fig. 1 add damping to the system, which is in benefit of the stability. The control design shown in the next section neglects such parasitic resistors, making the problem

more challenging as the damping must be provided only by the controller. Notice that the third-order state-space representation of the system model (1) - (3) is a linear system. Therefore, it admits a transfer function representation, which governs the open-loop performance, facilitates the design of the LCL filter, and allows the computation of its resonant frequency. This information is then used to suggest a switching frequency where the inverter can operate normally. If R_1 and R_2 are neglected, then the transfer functions $G_{I_1}(s)= I_1(s)/E(s)$, $G_{I_S}(s)=I_S(s)/E(s)$ and $G_{V_C}(s)=V_C(s)/E(s)$ are given by:

$$G_{I_1}(s)=\left[s^2+1/(L_2C)\right]\Big/\left(L_1\Delta(s)\right) \tag{4}$$

$$G_{I_S}(s)=1\Big/\left(L_1L_2C\Delta(s)\right) \tag{5}$$

$$G_{V_C}(s)=s\Big/\left(L_1C\Delta(s)\right) \tag{6}$$

where the characteristic polynomial $\Delta(s)$ and resonance frequency ω_{res} are given by:

$$\begin{cases}\Delta(s)=s^3+\left(\dfrac{L_1+L_2}{L_1L_2C}\right)s\\ \omega_{res}=\sqrt{\dfrac{L_1+L_2}{L_1L_2C}}\end{cases} \tag{7}$$

A common design of the LCL filter, intended to mitigate switching frequency components and to reduce the filter size [2], [22], [23], consists in computing the minimum value of L_1 to guarantee the required inverter-side current ripple. Afterwards, the LCL filter capacitor C is selected based on the maximum reactive power handled by the capacitor. It is common in practice to fix the reactive power handled by C between 5% and 15% of the rated active power supplied to the grid. However, a compromise arises between the amount of the capacitor reactive power and the filter ability to attenuate the switching ripple. On one hand, if the capacitance is large, the handled reactive power is large as well. On the other hand, if the capacitance is small, the attenuation ability of the LCL filter diminishes. Finally, the grid-side inductor value is selected to meet the required ripple attenuation at the grid-side current, and also to locate the LCL resonance frequency ω_{res} in (7) between $10\omega_S$ and πf_{sw}.

III. Analysis and Control Design

This section presents the design of the inverter-side current controller to achieve active damping for the LCL grid connected inverter. The controller is based on the inverter-side current feedback to damp the system resonance. It includes a proportional term over the inverter-side current error. Therefore, an appropriate design of the inverter-side current reference is essential to accomplish the main control objective, i.e., to compel a proper grid-side current. A resonant control structure [24], [25] is also included in the controller, which operates on the inverter-side current error as well. The aim of the resonant structure is to compensate harmonic distortion that may be present in the grid, which is well supported by the internal model principle [26]. It is worth mentioning that the controller addressed herein requires a reduced number of sensors. In fact, only grid voltage and inverter-side current are measured. The design of the controller is presented in the following subsections. First, the current error feedback is addressed, and the arguments on stability and dynamics are presented. Second, the computation of the inverter-side current reference is presented, which relies on the estimation of the fundamental frequency component of the grid voltage and its square-phase companion. An analysis of the steady state of the current reference computation scheme is performed to bound the error that arises when the grid voltage has harmonic distortion. Finally, a resonant control structure is introduced to compensate grid frequency harmonics.

A. Current Error Feedback

In this section, the error system is obtained by considering an output feedback, where only the inverter-side current is measured. The controller consists of a proportional gain for which an stability analysis is performed. A resonant control structure is added to the main controller to deal with possibly harmonic distortion in the grid voltage.

The controller operates on the inverter-side current error, which is the difference between the measured and an appropriately designed reference of the inverter-side current. The following assumptions are considered to simplify the error dynamics in the controller derivation.

1) The grid fundamental frequency has a known constant value of $f_S=\omega_S/(2\pi)$.

2) Parasitic resistors R_1 and R_2 have an arbitrarily small value and can be neglected in the system dynamics (1)-(3).

If ω_S is unknown, an estimator such as the one presented in [27] can be used. Notice that the second assumption above poses a more challenging control problem, as the missing damping must be introduced only by the controller.

To supply only active power to the grid, i_S must asymptotically track a reference i_S^{ref}, which is composed of fundamental components only and is in phase with the grid voltage. The amplitude of i_S^{ref} is proportional to the amount of power to be supplied to the grid, namely, the power reference P_{ref}. This control objective is denoted by $i_S\to i_S^{ref}$ as $t\to\infty$, and must be fulfilled with uniform stability.

Consider i_S^{ref} to be an admissible trajectory for i_1, then i_1, v_C, and e track references i_1^{ref}, v_C^{ref}, and e^{ref}, respectively, which are governed by system dynamics (1)-(3). Define the error state variables as $\tilde{i}_1=i_1-i_1^{ref}$, $\tilde{i}_S=i_S-i_S^{ref}$, $\tilde{v}_C=v_C-v_C^{ref}$ and $u=e-e^{ref}$. Based on these error definitions, the system (1)-(3) is transformed into the following system, which is referred to as the error system:

$$L_1\,\mathrm{d}\tilde{i}_1/\mathrm{d}t=-\tilde{v}_C+u \tag{8}$$

$$L_2 \mathrm{d}\tilde{i}_S/\mathrm{d}t = \tilde{v}_C \tag{9}$$

$$C\mathrm{d}\tilde{v}_C/\mathrm{d}t = \tilde{i}_1 - \tilde{i}_S \tag{10}$$

The system described in (8)-(10) is linear and time-invariant, and has a pole at the origin and two complex conjugate poles. The magnitude of the latter equals the resonant frequency ω_{res} in (7). In order to fulfill the control objective, the above error system must have the origin as an asymptotically stable equilibrium point. Then, the following controller is proposed, which relies on the feedback of $\tilde{i}_1$, which is expressed in (11).

$$u = -k\tilde{i}_1 \tag{11}$$

where k is a strictly positive constant gain. The closed-loop error system (8)-(11) can be rewritten in the form of an autonomous system as follows:

$$\boldsymbol{Q}\mathrm{d}\tilde{\boldsymbol{x}}/\mathrm{d}t = \tilde{\boldsymbol{A}}\tilde{\boldsymbol{x}} \tag{12}$$

$$\boldsymbol{Q}\mathrm{d}\tilde{\boldsymbol{x}}/\mathrm{d}t = \begin{bmatrix} -k & 0 & -1 \\ 0 & 0 & 1 \\ 1 & -1 & 0 \end{bmatrix}\tilde{\boldsymbol{x}} \tag{13}$$

where $\boldsymbol{Q} = \mathrm{diag}(L_1, L_2, C)$ is the diagonal matrix with filter parameters in its diagonal, and the error state vector is given by $\tilde{\boldsymbol{x}} = [\tilde{i}_1, \tilde{i}_S, \tilde{v}_C]^{\mathrm{T}}$. The closed-loop state matrix is given by (14).

$$\boldsymbol{Q}^{-1}\tilde{\boldsymbol{A}} = \boldsymbol{Q}^{-1}\begin{bmatrix} -k & 0 & -1 \\ 0 & 0 & 1 \\ 1 & -1 & 0 \end{bmatrix} \tag{14}$$

The model in (13) represents the closed-loop error average model in time domain with inverter-side current error feedback. The roots of its closed-loop characteristic polynomial in the frequency domain establishes stability. Closed-loop polynomial together with the related transfer function is used to prove closed-loop stability with the inverter-side current error feedback by appealing to the root locus method. The filter inductor ratio is defined by $\alpha = L_2/L_1$. Then the closed-loop characteristic polynomial is given by (15) and its roots are the closed-loop poles, or equivalently, the eigenvalues of $\boldsymbol{Q}^{-1}\tilde{\boldsymbol{A}}$.

$$\Delta_{cl}(s) = s^3 + \frac{1+\alpha}{\alpha L_1 C}s + k\left(\frac{1}{L_1}s^2 + \frac{1}{\alpha L_1^2 C}\right) \tag{15}$$

Then, the closed-loop poles coincide with the solutions of $1 + kG(s) = 0$, where $G(s)$ is expressed in (16).

$$G(s) = \frac{\dfrac{1}{L_1}s^2 + \dfrac{1}{\alpha L_1^2 C}}{s^3 + \dfrac{1+\alpha}{\alpha L_1 C}s} \tag{16}$$

The open-loop poles of $G(s)$ are located at zero and at $\pm\mathrm{j}\sqrt{(1+\alpha)/(\alpha L_1 C)}$, and the zeros at $\pm\mathrm{j}\sqrt{1/(\alpha L_1 C)}$. The root locus of the closed-loop poles as a function of gain k, which varies from zero to infinity, may adopt either of the sketches shown in Fig. 2. For $k = 0$, the closed-loop poles coincide with the open-loop poles. As k increases, the closed-loop poles follow the root loci of Fig. 2. The value of the inductor ratio $\alpha = L_2/L_1$ relative to 8 determines the behavior of the root loci as k varies. Figure 2 shows that if the gain k is positive, then the closed-loop poles have negative real parts, which guarantees closed-loop stability. Additionally, the value $\alpha = L_2/L_1$ differentiates the performance of several stable closed-loop systems. This has an effect on the performance of the transient response rather than on the stability. In practice, the case $\alpha = 8$ or even $\alpha > 8$ rarely appears. In fact, L_1 is usually designed to be larger than L_2 as the inverter-side current gets larger switching ripple. If $\alpha \geq 8$, then there exist break-in or breakaway points of the closed-loop poles to the real line as observed in Fig. 2(b) and Fig. 2(c). This is not the case for $\alpha < 8$ as shown in Fig. 2(a). That is, for $\alpha \geq 8$, there are discrete values of k for which multiple closed-loop real poles occur. Such values of k can be obtained by solving the critical points of function $f(s) = 1 + kG(s)$ [28].

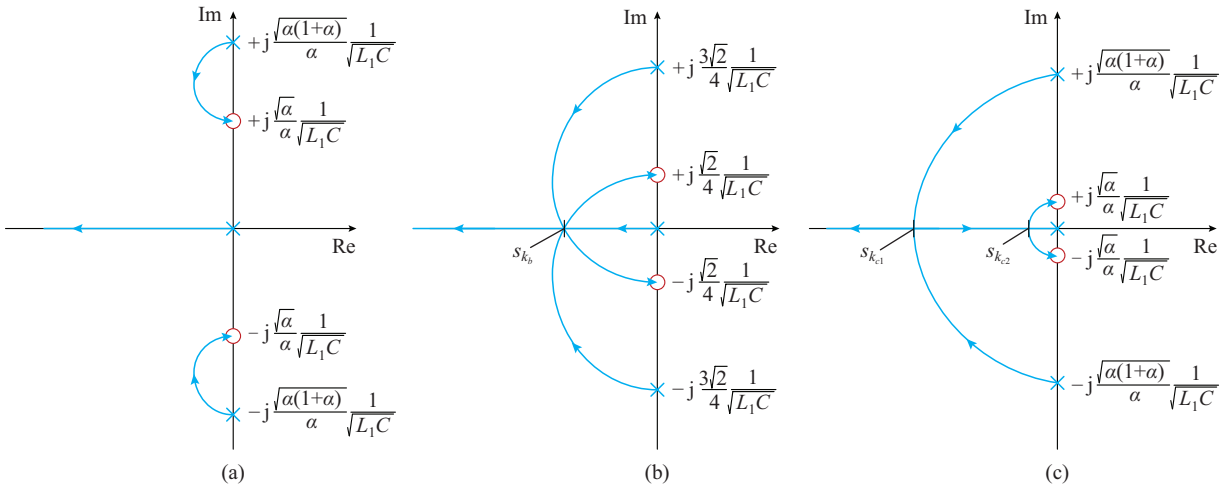

Fig. 2. General forms of root-locus for inverter-side current error feedback loop. (a) $L_2 < 8L_1$. (b) $L_2 = 8L_1$. (c) $L_2 > 8L_1$.

If $\alpha<8$, $L_2<8L_1$, and the root locus is depicted in Fig. 2 (a) where one closed-loop pole has negative real part for any $k>0$ and tends to a zero at $-\infty$ as $k\to\infty$. The two remaining closed-loop poles are complex conjugates with negative real part for any $k>0$, and tend to the zeros located in the imaginary axis at $\pm j\sqrt{1/(L_2C)}$ as $k\to\infty$. This is a typical root locus that ocurrs when the value of the inverter-side inductor is larger than that of the grid-side inductor. This selection is done by considering that the switching harmonic content is larger in the inverter-side current than in the grid-side current.

If $\alpha=8$, $L_2=8L_1$, and the root locus is shown in Fig. 2(b). In this case, there is one negative real closed-loop pole that tends to the zero located at $-\infty$, and there are two closed-loop poles that have negative real part and tend to the zeros located in the imaginary axis at $\pm j(\sqrt{2}/4)\sqrt{1/(L_1C)}$. There is a point in the real line $s_{k_b}=-(\sqrt{6}/4)\sqrt{1/(L_1C)}$ as shown in Fig. 2(b), where the three closed-loop poles coincide with feedback gain k_b expressed in (17).

$$k_b=\frac{3\sqrt{6}}{4}\sqrt{\frac{L_1}{C}} \tag{17}$$

If $\alpha>8$, $L_2>8L_1$, and the root locus is shown in Fig. 2(c). One closed-loop pole is real and tends to $-\infty$ when $k\to\infty$. The other two closed-loop poles have negative real part and tend to the zeros located at $\pm j(\sqrt{\alpha}/\alpha)\sqrt{1/(L_1C)}$ in the imaginary axis as $k\to\infty$. However, for the subset of gains $[k_{c1},k_{c2}]\subset\mathbf{R}$, all closed-loop poles become negative real. The gains k_{c1} and k_{c2} are expressed in (18).

$$\begin{cases} k_{c1}=\dfrac{\sqrt{2\alpha(\alpha-2)+\sqrt{\alpha(\alpha-8)}}}{2\alpha}\dfrac{3\alpha+\sqrt{\alpha(\alpha-8)}}{\alpha+\sqrt{\alpha(\alpha-8)}}\sqrt{\dfrac{L_1}{C}} \\ k_{c2}=\dfrac{\sqrt{2\alpha(\alpha-2)-\sqrt{\alpha(\alpha-8)}}}{2\alpha}\dfrac{3\alpha-\sqrt{\alpha(\alpha-8)}}{\alpha-\sqrt{\alpha(\alpha-8)}}\sqrt{\dfrac{L_1}{C}} \end{cases} \tag{18}$$

There exists an entry/exit to/from the real line of the complex conjugated closed-loop poles, occurring at $s_{k_{c1}}$ and $s_{k_{c2}}$, respectively, expressed in (19).

$$\begin{cases} s_{k_{c1}}=-\dfrac{\sqrt{2\alpha(\alpha-2+\sqrt{\alpha(\alpha-8)})}}{2\alpha\sqrt{L_1C}} \\ s_{k_{c2}}=-\dfrac{\sqrt{2\alpha(\alpha-2-\sqrt{\alpha(\alpha-8)})}}{2\alpha\sqrt{L_1C}} \end{cases} \tag{19}$$

From this analysis, it can be concluded that, for any of the possible cases with $k>0$, the asymptotic stability of the origin is guaranteed since closed-loop poles have negative real parts. However, the transient response depends on different ratios α and feedback gains k. Therefore, the inverter-side current feedback (11) adds active damping by moving the closed-loop poles to the left-side of the complex plane as the gain parameter k increases. For a relatively small k, the response is dominated by the real closed-loop pole closest to the origin, where the response is well damped. For a relatively large value of k, the response behavior is dominated by complex conjugated closed-loop poles, which dictates an oscillatory behavior of the closed-loop system. In either case, an increase in gain $k>0$, in a given range, causes the reduction of the imaginary part of the complex conjugated closed-loop poles in each of the cases depicted in Fig. 2. As a consequence, a more damped behavior is expected, with a damping coefficient depending on the system parameters.

Therefore, with the inverter-side current feedback (11), and taking into consideration the inverter voltage reference e^{ref}, the inverter voltage $e=u+e^{ref}$ is given by (20).

$$e=-k\tilde{i}_1+e^{ref} \tag{20}$$

Under the above assumptions, the feedback controller (20) renders the closed-loop system stable. The computation of e requires i_1^{ref} and e^{ref}, where e^{ref} can be seen as a decoupling term. The next subsection presents a method to obtain estimates of i_1^{ref} and e^{ref}, in the case where the grid voltage and i_S^{ref} are pure sinusoidal signals, i.e., contain fundamental component only. The case with harmonic distortion in the grid voltage requires a harmonic compensation mechanism, which is presented right after the next subsection.

B. Definition and Estimation of Admissible Reference

Implementation of the above controller (20) requires the reference i_1^{ref} and the decoupling term e^{ref} to accomplish the control objective, i.e., to assure that i_S is a pure sinusoidal signal with the same frequency and phase of the fundamental component of v_S. This subsection presents the estimation for these two references. For the ease of presentation, this subsection considers the case of a pure sinusoidal v_S, which is composed of fundamental component only. It is proved that the estimates $\hat{i}_1^{ref}$ and $\hat{e}^{ref}$ converge towards their references i_1^{ref} and e^{ref}, respectively, in the steady state. However, in the presence of harmonic distortion in v_S, the reference estimations exhibit a bounded convergence error.

If the grid voltage v_S has no harmonic distortion, the grid-side current reference can be computed in terms of v_S, and the desired active power to be supplied to the grid P_{ref}. However, in general conditions, v_S has additional harmonic components, and therefore, its fundamental component may be used instead. Let $v_{S,1}$ be the steady-state fundamental component of the grid voltage, and $\phi_{v_{S,1}}$ be its square-phase companion, that is, $\phi_{v_{S,1}}$ coincides with $v_{S,1}$ except for a phase shift difference of 90°. Notice that $v_{S,1}$ and $\phi_{v_{S,1}}$ form a basis for the set of periodic signals at the fundamental grid frequency. Therefore, the system references $i_1^{ref}, i_S^{ref}, v_C^{ref}$ and e^{ref} in steady state can be constructed as linear combinations of $v_{S,1}$ and $\phi_{v_{S,1}}$.

To guarantee the fulfillment of the control objective, i_S must be proportional to $v_{S,1}$, whose amplitude is fixed by the

desired active power to be supplied. Let $g=P_{ref}/V_{S,RMS}^2$ be the apparent conductance of the system, and $V_{S,RMS}$ the root-mean-square (RMS) value of the grid voltage. Then the grid-current reference can be proposed as (21).

$$i_S^{ref}=gv_{S,1} \tag{21}$$

Let $\boldsymbol{x}^{ref}=[i_1^{ref},i_S^{ref},v_C^{ref}]^{\mathrm{T}}$, then the remaining system references are imposed by the system dynamics (1)-(3), and can be expressed by (22).

$$\boldsymbol{x}^{ref}=\begin{bmatrix} g\left(1-\omega_S^2L_2C\right) & \omega_SC \\ g & 0 \\ 1 & g\omega_SL_2 \end{bmatrix}\begin{bmatrix} v_{S,1} \\ \phi_{v_{S,1}} \end{bmatrix} \tag{22}$$

Moreover, the admissible steady-state inverter voltage is given by (23).

$$e^{ref}=\left(1-\omega_S^2L_1C\right)v_{S,1}+g\omega_S\left(L_1+L_2-\omega_S^2L_1L_2C\right)\phi_{v_{S,1}} \tag{23}$$

Notice that $v_{S,1}$ and $\phi_{v_{S,1}}$ satisfy (24).

$$\begin{bmatrix} \mathrm{d}v_{S,1}/\mathrm{d}t \\ \mathrm{d}\phi_{v_{S,1}}/\mathrm{d}t \end{bmatrix}=\begin{bmatrix} 0 & \omega_S \\ -\omega_S & 0 \end{bmatrix}\begin{bmatrix} v_{S,1} \\ \phi_{v_{S,1}} \end{bmatrix} \tag{24}$$

The time-derivative of the system state reference (22) is given by (25).

$$\mathrm{d}\boldsymbol{x}^{ref}/\mathrm{d}t=\begin{bmatrix} -\omega_SC & g\omega_S\left(1-\omega_S^2L_2C\right) \\ 0 & g\omega_S \\ -g\omega_S^2L_2 & \omega_S \end{bmatrix}\begin{bmatrix} v_{S,1} \\ \phi_{v_{S,1}} \end{bmatrix} \tag{25}$$

Based on (22) and the above time-derivative, it can be verified that references in (22) satisfy the system dynamics (1)-(3), and thus, they are admissible trajectories.

The following linear, uniformly stable estimator for the fundamental component of the grid voltage $\tilde{v}_{S,1}$ and of its square-phase companion $\tilde{\phi}_{v_{S,1}}$ is used based on the linear estimator presented in [24], [29], [30].

$$\mathrm{d}\tilde{v}_{S,1}/\mathrm{d}t=\lambda\left(v_S-\tilde{v}_{S,1}\right)+\omega_S\phi_{v_{S,1}} \tag{26}$$

$$\mathrm{d}\tilde{\phi}_{v_{S,1}}/\mathrm{d}t=-\omega_S\tilde{v}_{S,1} \tag{27}$$

The estimation gain $\lambda>0$ modifies the rate of the estimation. Estimates of $\hat{i}_1^{ref}$ and of $\hat{e}^{ref}$ can be computed as follows:

$$\hat{i}_1^{ref}=g\left(1-\omega_S^2L_2C\right)\tilde{v}_{S,1}+\omega_SC\phi_{v_{S,1}} \tag{28}$$

$$\hat{e}^{ref}=\left(1-\omega_S^2L_1C\right)\tilde{v}_{S,1}+g\omega_S\left(L_1+L_2-\omega_S^2L_1L_2C\right)\phi_{v_{S,1}} \tag{29}$$

If reactive power injection is required, references (28) and (29) can be modified as follows. Let Q_{ref} be the desired reactive power references, and define $h=Q_{ref}/V_{S,RMS}^2$. The magnitude of the apparent admittance of the system is define as $\sqrt{g^2+h^2}$. Then the required grid current reference in (21) must be modified to $i_S^{ref}=gv_{S,1}+h\phi_{v_{S,1}}$. Following an analogous procedure as the one used to obtain the references imposed by the system dynamics (22) and the admissible steady-state inverter voltage (23), the following references can be proposed.

$$\hat{i}_{1,PQ}^{ref}=\hat{i}_1^{ref}+h(1-\omega_S^2L_2C)\phi_{v_{S,1}} \tag{30}$$

$$\hat{e}_{PQ}^{ref}=\hat{e}^{ref}-h\omega_S(L_1+L_2-\omega_S^2L_1L_2C)\tilde{v}_{S,1} \tag{31}$$

Then, the expressions (30) and (31) are the estimated references for the inverter-side inductor current and the steady-state inverter voltage, respectively, when the reactive power reference Q_{ref} is not zero.

In fact, the estimator in (26) and (27) is linear. Its eigenvalues have negative real part, and it is bounded-input, bounded-output stable. Therefore, if the grid voltage is bounded and periodic, the estimations $\hat{i}_1^{ref}$ and $\hat{e}^{ref}$ are also bounded and periodic.

Assuming that v_S has no harmonic contents, the estimations $\hat{i}_1^{ref}$ and $\hat{e}^{ref}$ in (28) and (29) converge exponentially toward i_1^{ref}, in the first scalar equation of (22), and e^{ref} in (23). However, if v_S has considerable harmonic contents, there is an steady-state error between estimated references and actual references. In the remaining part of this subsection, bounds are obtained for these errors. The usual grid voltage harmonics for single-phase electrical systems are at odd multiples of the fundamental frequency. Then the Fourier series representation of the grid voltage in steady-state is expressed as $v_S=\sum_{n=1}^{\infty}V_{m,2n-1}\sin\left((2n-1)\omega_St-\varphi_{2n-1}\right)$. Notice that $\hat{I}_1^{ref}(s)=G_1(s)V_S(s)$ and $\hat{E}^{ref}(s)=G_2(s)V_S(s)$, where $G_1(s)$ and $G_2(s)$ are given in (32).

$$\begin{cases} G_1(s)=\dfrac{\lambda g\left(1-\omega_S^2L_2C\right)s-\lambda\omega_S^2C}{s^2+\lambda s+\omega_S^2} \\ G_2(s)=\dfrac{\lambda\left(1-\omega_S^2L_1C\right)s-\lambda g\omega_S^2\left(L_1+L_2-\omega_S^2L_1L_2C\right)}{s^2+\lambda s+\omega_S^2} \end{cases} \tag{32}$$

The magnitudes of these transfer functions at each consecutive multiple n of the harmonic frequency, i. e., $M_1(n)=|G_1(\mathrm{j}(2n-1)\omega_S)|$ and $M_2(n)=|G_2(\mathrm{j}(2n-1)\omega_S)|$ are given by (33), where $n\in\mathbb{N}^+$.

$$\begin{cases} M_1(n)=\dfrac{\lambda\sqrt{g^2\left(1-\omega_S^2L_2C\right)^2(2n-1)^2+\omega_S^2C^2}}{\sqrt{\lambda^2(2n-1)^2+16n^2(n-1)^2\omega_S^2}} \\ M_2(n)=\dfrac{\lambda\sqrt{g^2\omega_S\left(L_1+L_2-\omega_S^2L_1L_2C\right)^2+(2n-1)^2(1-\omega_SL_1C)}}{\sqrt{\lambda^2(2n-1)^2+16n^2(n-1)^2\omega_S^2}} \end{cases} \tag{33}$$

Therefore, the Fourier representation of the steady-state estimated references are given by (34).

$$\begin{cases} \hat{i}_1^{ref}=\sum_{n=1}^{\infty}V_{m,2n-1}M_1(n)\sin\left((2n-1)\omega_St-\psi_{2n-1}\right) \\ \hat{e}^{ref}=\sum_{n=1}^{\infty}V_{m,2n-1}M_2(n)\sin\left((2n-1)\omega_St-\theta_{2n-1}\right) \end{cases} \tag{34}$$

where $\psi_{2n-1}=\varphi_{2n-1}-\angle G_1(\mathrm{j}(2n-1)\omega_S)$ and $\theta_{2n-1}=\varphi_{2n-1}-$

$\angle G_1(\mathrm{j}(2n-1)\omega_S)$. Hence, the error of each estimated reference, $\Delta i_1^{ref} = \hat{i}_1^{ref} - i_1^{ref}$ and $\Delta e^{ref} = \hat{e}^{ref} - e^{ref}$, satisfy (35) and (36).

$$|\Delta i_1^{ref}| \le \frac{\lambda\omega_S C}{4}\sum_{n=2}^{\infty}\frac{V_{m,2n-1}}{n(n-1)} + \frac{\lambda g|1-\omega_S^2 L_1 C|}{4}\sum_{n=2}^{\infty}\frac{V_{m,2n-1}}{n} \quad (35)$$

$$|\Delta e^{ref}| \le \frac{\lambda g\omega_S|L_1+L_2-\omega_S^2 L_1 L_2 C|}{4}\sum_{n=2}^{\infty}\frac{V_{m,2n-1}}{n(n-1)} + \frac{\lambda|1-\omega_S^2 L_1 C|}{4}\sum_{n=2}^{\infty}\frac{V_{m,2n-1}}{n} \quad (36)$$

If the harmonic components of v_S are zero from a given n and above, as occurs in practical applications, or if the magnitude of the harmonics is of the order of $1/n$, errors are bounded since the sums in the inequalities (35) and (36) are convergent. The approximation error becomes zero whenever the grid voltage is a pure sinusoidal.

C. Harmonic Compensation Mechanism

The harmonic distortion of v_S propagates to the controller and estimator. A solution to compensate the harmonic distortion is to use a resonant control structure following the principle of the internal model [26]. This includes the model of the perturbation to be compensated in the stable feedback path. Hence, asymptotic tracking is achieved. This control approach has been successfully used in several power electronics applications [24], [25].

Considering the estimated references $\hat{i}_1^{ref}$ and $\hat{e}^{ref}$, the controller (20) can be expressed as follows:

$$e = -ki_1 + k\hat{i}_1^{ref} + \hat{e}^{ref} - ki_1 + k\left(i_1^{ref} - \Delta i_1^{ref}\right) + \left(e^{ref} - \Delta e^{ref}\right) - ki_1 + ki_1^{ref} + e^{ref} + \Phi \quad (37)$$

where $\Phi = -k\Delta i_1^{ref} - \Delta e^{ref}$ is a periodic bounded perturbation whose Fourier series representation includes the odd harmonics in the grid voltage. Therefore, a resonant control structure may be included at the feedback path to compensate Φ, which consists of a set of resonant filters tuned at odd multiples of the fundamental grid frequency, i.e., frequencies defined by $(2n-1)\omega_S$, $\forall n \in \{1, 2, \cdots, N\}$, where N can be fixed as the number of the first more significant harmonics in the grid voltage. By considering the resonant structure (37), the following expression for the controller is obtained:

$$e = -ki_1 + ki_1^{ref} + e^{ref} + \Phi - \sum_{n=1}^{N}\gamma_{2n-1}\zeta_{2n-1} \quad (38)$$

The last term in (38) can be implemented in the form of a transfer function as follows:

$$\sum_{n=1}^{N}\gamma_{2n-1}\zeta_{2n-1}(s) = \sum_{n=1}^{N}\frac{\gamma_{2n-1}s}{s^2+(2n-1)^2\omega_S^2} \quad (39)$$

where γ_{2n-1}, $\forall n \in \{1, 2, \cdots, N\}$ is a constant gain.

A block diagram of the overall controller is presented in Fig. 3. The inputs of the reference estimation block are v_S and P_{ref}, and the generated outputs are the $\hat{e}^{ref}$ and $\hat{i}_1^{ref}$ described by (28) and (29), respectively. The parameters g, $a_1 = 1-\omega_S^2 L_1 C$, $a_2 = 1-\omega_S^2 L_2 C$, $a_3 = \omega_S C$ and $a_4 = \omega_S\left(L_1 + L_2 - \omega_S^2 L_1 L_2 C\right)$ are involved in the calculation of the estimates. The inputs of the controller are the inverter-side current, the inverter-side current reference and the estimations coming from the reference estimation block. The controller includes two actions namely proportional and resonant control actions over the inverter-side current error. To avoid issues caused by the infinite gain at resonant peaks, it is proposed to implement the bank of resonant filters (39) as follows:

$$\sum_{n=1}^{N}\frac{\gamma_{2n-1}\left[(2n-1)\omega_S/Q_{2n-1}\right]s}{s^2+\left[(2n-1)\omega_S/Q_{2n-1}\right]s+(2n-1)^2\omega_S^2} \quad (40)$$

where the resonant filters have been replaced by selective band-pass filters. These filters have an adjustable limited gain γ_{2n-1}, and can be made as selective as required through the quality factor Q_{2n-1}.

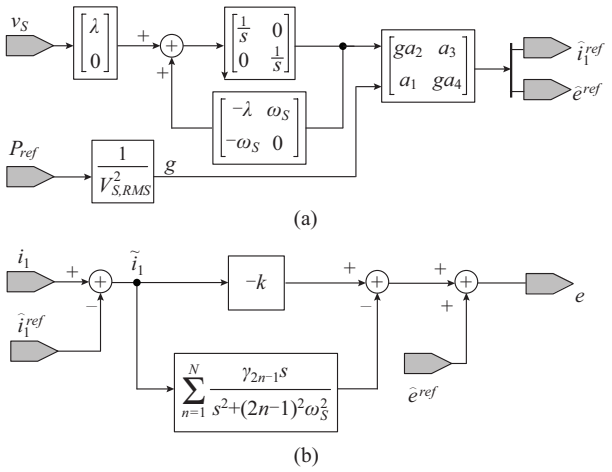

Fig. 3. Block diagram of reference estimation and feedback controller. (a). Reference estimation. (b). Feedback controller.

IV. Experimental Validation

The controller presented in Fig. 3 is experimentally tested to evaluate its performance in a 1.0 kVA HB prototype built upon insulated gate bipolar transistor (IGBT) modules and with unipolar sinusoidal pulse width modulation (SPWM). The controller is not limited to this particular topology, and can be modified to control other single-phase topologies. The inverter is connected to the local grid, with an RMS voltage of 122 V, $\omega_S = 120\pi$ rad/s, through an LCL filter. The power is supplied by a programmable DC voltage source. The experimental setup is shown in Fig. 4. It includes current and voltage sensors, a signal conditioning stage, a power stage and a dSPACE ACE 1103 control board where the controller is implemented. It is worth mentioning that the proposed controller can also be implemented in a DSP-based control board. This is possible because the control strategy involves common math operations and second-order transfer functions (for the reference estimation block and for each harmonic to compensate).

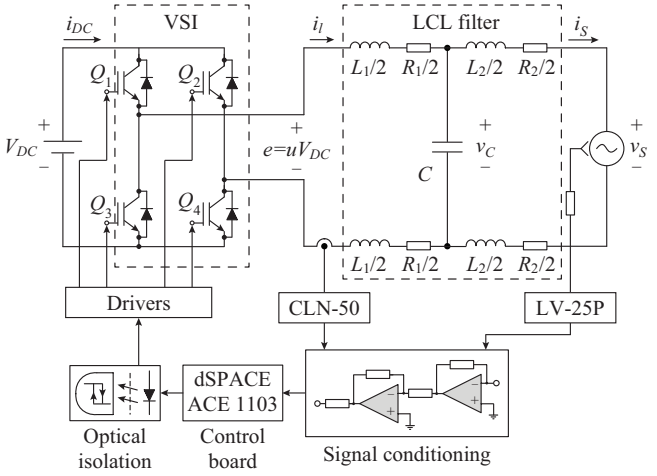

Fig. 4. LCL grid-connected power inverter experimental setup.

The DC-link voltage is fixed to $V_{DC}=240$ V, the switching frequency is set to $f_{sw}=8$ kHz, and the power reference is set to $P_{ref}=700$ W, which is the active power to be supplied to the grid. The LCL filter parameters are $L_1=1$ mH, $L_2=552$ μH, $C=8$ μF. The sampling period is 50 μs. Other system and controller parameters are $V_{S,RMS}=127$ V, $k=6.5$, $\lambda=250$, $a_1=0.9988$, $a_2=0.9994$, $a_3=3.016\times10^{-3}$, $a_4=0.5848$, $\gamma_1=96$, $Q_1=93$, $\gamma_3=93$, $Q_3=94$, $\gamma_5=92$, $Q_5=90$, $\gamma_7=99.89$, $Q_7=92.37$, $\gamma_9=71$, $Q_9=92$, $\gamma_{11}=50$, $Q_{11}=88$, $\gamma_{13}=9.54$, $Q_{13}=89$, $\gamma_{15}=21$, $Q_{15}=61$, $\gamma_{17}=65$, $Q_{17}=77$.

The above parameters follow the design rules previously presented and reported in [2], [22], [23]. However, for the sake of completeness, the tuning process is described in more detail as follows. The base capacitance and base inductance are given by $C_b=P_{ref}/(\omega_S V_{S,RMS}^2)=115.12$ μF and $L_b=V_{S,RMS}^2/(\omega_S P_{ref})=61.12$ mH, respectively. The maximum inverter-side current ripple is given by $\Delta I_{1,\max}=V_{DC}/(8L_1 f_{sw})=3.75$ A. The sum L_1+L_2 equals 1.552 mH, which is lower than the recommended 10% of L_b, i.e., it is lower than 6.11 mH. The filter capacitance $C=8$ μF does not exceed the recommended 15% of C_b, i.e., it is lower than 17.26 μF. This value limits the reactive power demanded by the LCL filter capacitor. The LCL resonance frequency $f_{res}=\sqrt{(L_1+L_2)/(L_1L_2C)}\big/2\pi$ is located at 2.984 kHz, which lies between ten times the grid frequency $f_S=60$ Hz and half the effective switching frequency at the inverter output. This is a common practice to avoid resonance issues in LCL-filter-based converter applications [31], [32].

The experiments include tests where the harmonic compensation block of the controller shown in Fig. 3 is enabled and disabled with the purpose to demonstrate its benefits, respectively. In both cases, only v_S and i_1 are measured. Two system responses are presented to evaluate the performance of the proposed controller, the steady-state response at $P_{ref}=700$ W, and the transient response during step changes of the power reference between 350 W and 700 W.

Figure 5 shows the steady-state responses at $P_{ref}=700$ W without and with harmonic compensation. Both sub-plots show v_S, $\hat{v}_{S,1}$, i_1, and i_S. Notice that $\hat{v}_{S,1}$ in both sub-plots has an almost pure sinusoidal waveform despite the harmonic distortion present in v_S.

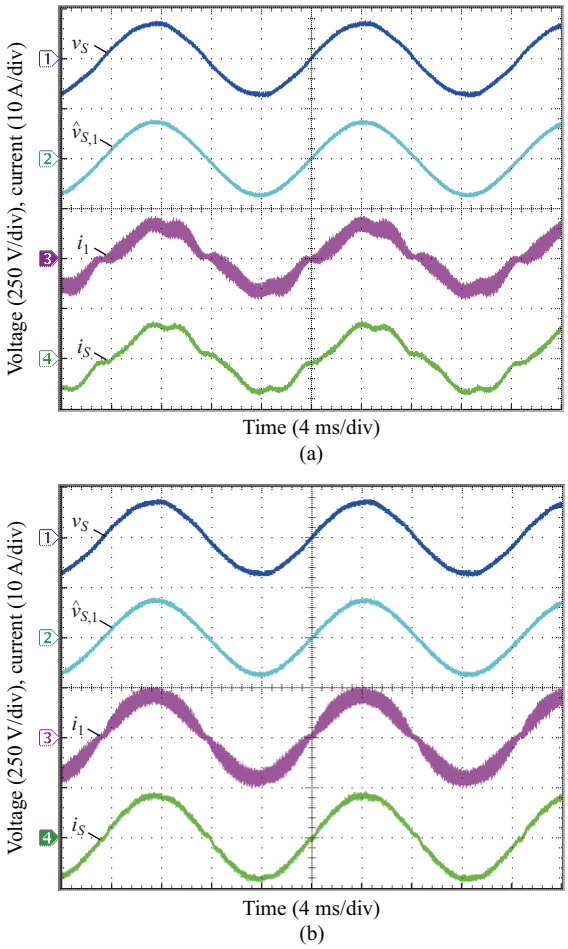

Fig. 5. Steady-state grid voltage, estimated grid voltage fundamental component, inverter-side current, and grid-side current with proposed controller considering $P_{ref}=700$ W. (a) Without harmonic compensation. (b) With harmonic compensation.

As observed in Fig. 5(a), if no harmonic compensation is included, both i_1 and i_S exhibit a slight harmonic distortion. In contrast, as observed in Fig. 5(b), if the harmonic compensation scheme is activated, both i_1 and i_S achieve almost pure sinusoidal waveforms, which corroborates the benefit of the compensation scheme. These figures also show the effectiveness of the LCL filter in reducing the switching harmonics at the grid-side current. Moreover, Fig. 5(b) shows that i_1^{ref} reaches an almost pure sinusoidal waveform with the required phase shift with respect to $\tilde{v}_{S,1}$. This is necessary to guarantee that i_S is in phase with the fundamental component of v_S.

Figure 6 shows the steady-state responses of the inverter-side current error $\tilde{i}_1$, the estimated inverter-side current reference $\hat{i}_1^{ref}$ and the inverter-side current i_1 at $P_{ref}=700$ W. Figure 6(a) shows the responses without harmonic compensa-

tion, while Fig. 6(b) shows the responses with harmonic compensation. It can be observed that $\hat{i}_1^{ref}$ is appropriately generated in both cases with and without the compensation scheme. As observed in Fig. 6(b), if the compensation mechanism is activated, i_1 achieves an almost sinusoidal waveform, and the amplitude of $\tilde{i}_1$ is reduced to zero.

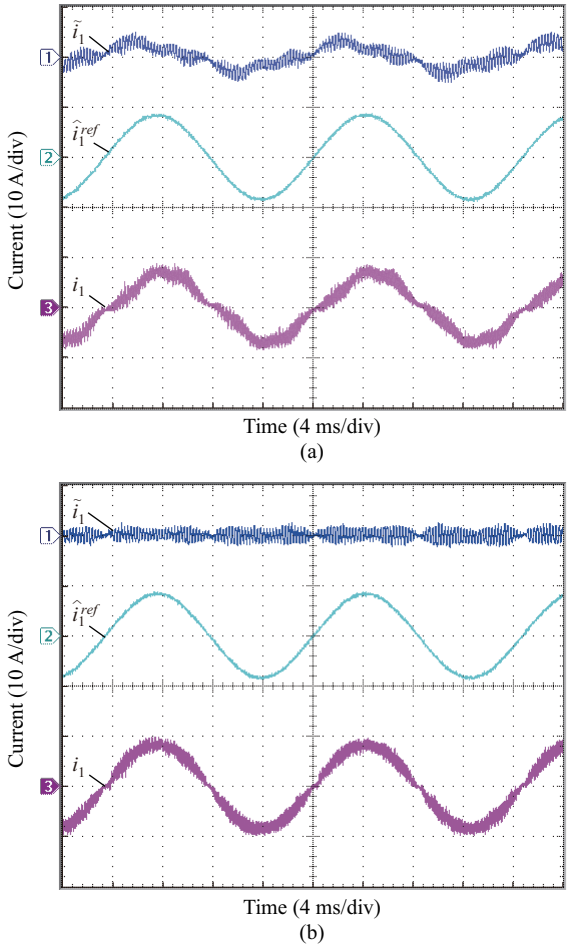

Fig. 6. Steady-state inverter-side current error, estimated inverter-side current reference, and inverter-side current, with proposed controller considering $P_{ref} = 700$ W. (a) Without harmonic compensation. (b) With harmonic compensation.

Figure 7 depicts the steady-state response of v_S and its fast Fourier transform (FFT) $v_{S,FFT}$, and i_S and its FFT $i_{S,FFT}$ at $P_{ref} = 700$ W. It can be observed that v_S is composed of the fifth and seventh harmonic components besides the fundamental component, while i_S contains mainly fundamental component.

Figure 8 shows the steady-state response at $P_{ref} = 700$ W under the overall controller, i.e., including the harmonic compensation mechanism. The figure includes e, $\hat{e}^{ref}$, i_1 and $\hat{i}_1^{ref}$. Notice that in the closed-loop operation, both references $\hat{e}^{ref}$ and $\hat{i}_1^{ref}$ coincide with the actual injected voltage and the measured inverter-side current, respectively, except for a high-frequency switching component in the inverter-side current.

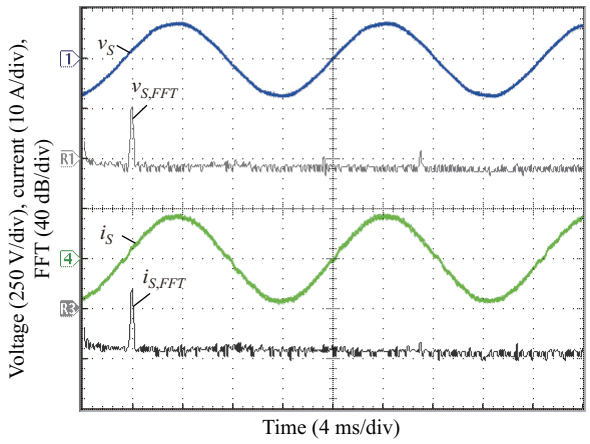

Fig. 7. Steady-state grid voltage and grid-side current with proposed controller (including harmonic compensation) and considering $P_{ref} = 700$ W (*x*-axis unit for FFT is 62.5 Hz).

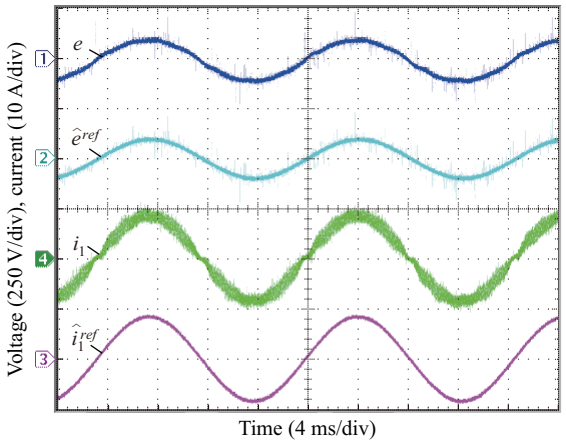

Fig. 8. Steady-state control voltage, estimated voltage reference, inverter-side current, and inverter-side current reference, with proposed controller (including harmonic compensation) and considering $P_{ref} = 700$ W.

The figure shows e, $\hat{e}^{ref}$, i_1 and $\hat{i}_1^{ref}$. Notice that the control voltage and the inverter-side current converge to their corresponding references in a relatively short time, without a noticeable overshoot nor settling time.

Figure 10 shows the transient responses with power step changes from 350 W to 700 W and back from 700 W to 350 W, with the overall controller. The figure shows P_{ref}, $\hat{i}_S^{ref}$, i_S and the grid-side current error $\tilde{i}_S = i_S - i_S^{ref}$. Notice that the current transients are relatively short as compared to the fundamental period of the grid voltage. In fact, both transients are very smooth without appreciable overshoots in the current time waveforms.

V. Conclusion

This paper presents the design, analysis and experimental validation of a model-based controller for a power inverter connected to the grid through an LCL filter, which has special interest in applications of photovoltaic generation systems among others.

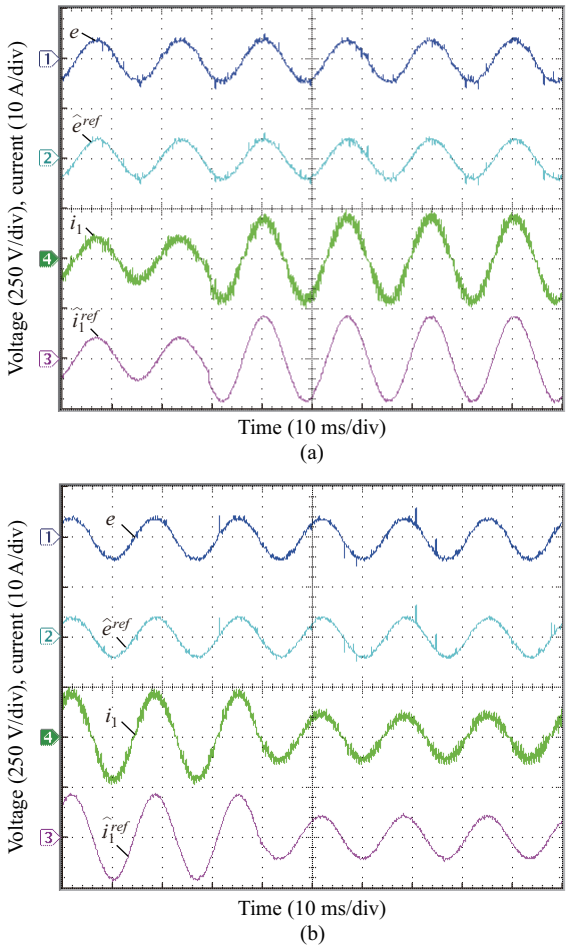

Fig. 9. Transient responses of control voltage, estimated voltage reference, inverter-side current, and inverter-side current reference in proposed scheme (including harmonic compensation) after power step changes. (a) Changing from 350 W to 700 W. (b) Back from 700 W to 350 W.

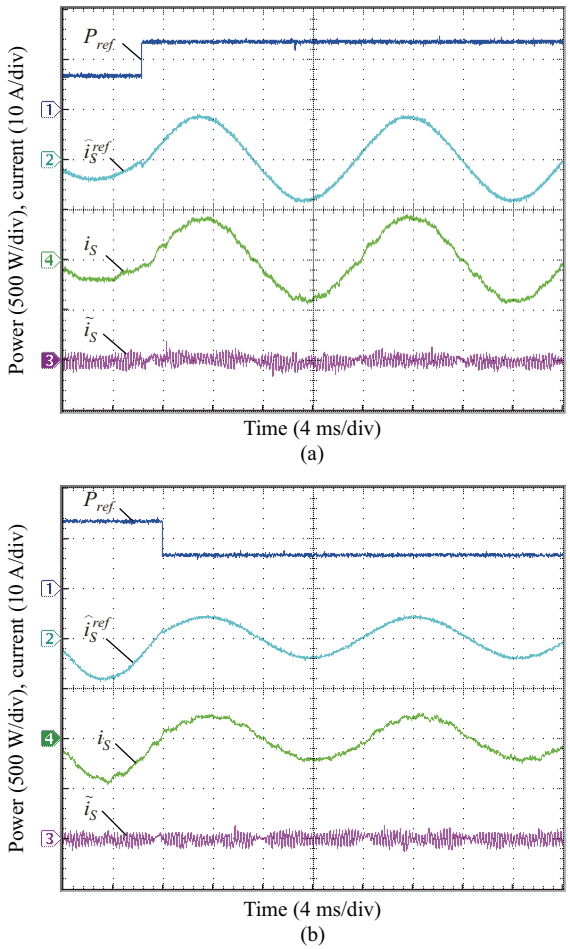

Fig. 10. Transient responses of power reference, grid-side current reference, grid-side current, and grid-side current error in proposed scheme (including harmonic compensation) after power step changes. (a) Changing from 350 W to 700 W. (b) Back from 700 W to 350 W.

The controller provides active damping and assures a grid-side current in phase with the fundamental component of the grid voltage. Moreover, the controller adopts a reduced number of measurements. In fact, only the grid voltage and the inverter-side current are required for the controller implementation. The controller structure consists of a proportional term and a harmonic compensation scheme over the inverter-side current error. One of the contributions of this work is the estimation of the inverter-side current reference and a decoupling term required for the controller implementation. Analysis has also been presented to show that the error between these estimations and the references turns out to be bounded. Moreover, it is shown that this error could be compensated even in the general case of a grid voltage with harmonic distortion. Therefore, the overall controller proposed in this paper is able to supply power to the grid with a guaranteed clean sinusoidal current signal. Experimental results with a laboratory prototype inverter prove the benefits of the proposed controller. The results show that the controller is able to introduce active damping and achieves lower-than-standard harmonic distortion in the grid-side current.

REFERENCES

[1] S. Kjaer, J. Pedersen, and F. Blaabjerg, "A review of single-phase grid-connected inverters for photovoltaic modules," *IEEE Transactions on Industry Applications*, vol. 41, no. 5, pp. 1292-1306, Sept.-Oct. 2005.

[2] M. Liserre, F. Blaabjerg, and A. Dell'Aquila, "Step-by-step design procedure for a grid-connected three-phase PWM voltage source converter," *International Journal of Electronics*, vol. 91, no. 8, pp. 445-460, Aug. 2004.

[3] Y. Riffonneau, S. Bacha, F. Barruel *et al*., "Optimal power flow management for grid connected PV systems with batteries," *IEEE Transactions on Sustainable Energy*, vol. 2, no. 3, pp. 309-320, Jul. 2011.

[4] J. M. Sosa, G. Escobar, P. R. Martinez-Rodriguez *et al*., "Control law for transformerless converters connected to the grid through an *L* filter," in *Proceedings of 2014 IEEE International Autumn Meeting on Power, Electronics and Computing (ROPEC)*, Ixtapa, Mexico, Nov. 2014, pp. 1-6.

[5] S. Li, X. Fu, M. Ramezani *et al*., "A novel direct-current vector control technique for single-phase inverter with L, LC and LCL filters," *Electric Power Systems Research*, vol. 125, pp. 235-244, Aug. 2015.

[6] J. Dannehl, M. Liserre, and F. W. Fuchs, "Filter-based active damping of voltage source converters with LCL filter," *IEEE Transactions on Industrial Electronics*, vol. 58, no. 8, pp. 3623-3633, Aug. 2011.

[7] G. Escobar, M. J. Lopez-Sanchez, D. F. Balam-Tamayo *et al*., "Inverter-side current control of a single-phase inverter grid connected through an LCL filter," in *Proceedings of 2014 40th Annual Conference of the IEEE Industrial Electronics Society (IECON)*, Dallas, USA, Oct.-Nov. 2014, pp. 1-7.

[8] X. Wang, C. Bao, X. Ruan *et al*., "Design considerations of digitally controlled LCL-filtered inverter with capacitor-current-feedback active

damping," *IEEE Journal of Emerging and Selected Topics in Power Electronics*, vol. 2, no. 4, pp. 972-984, Dec. 2014.
[9] R. N. Beres, X. Wang, M. Liserre *et al*., "A review of passive power filters for three-phase grid-connected voltage-source converters," *IEEE Journal of Emerging and Selected Topics in Power Electronics*, vol. 4, no. 1, pp. 54-69, Mar. 2016.
[10] V. Blasko and V. Kaura, "A novel control to actively damp resonance in input LC filter of a three-phase voltage source converter," *IEEE Transactions on Industry Applications*, vol. 33, no. 2, pp. 542-550, Mar.-Apr. 1997.
[11] Y. Tang, P. C. Loh, P. Wang *et al*., "Exploring inherent damping characteristic of LCL-filters for three-phase grid-connected voltage source inverters," *IEEE Transactions on Power Electronics*, vol. 27, no. 3, pp. 1433-1443, Mar. 2012.
[12] C. A. Busada, S. G. Jorge, and J. A. Solsona, "Full-state feedback equivalent controller for active damping in LCL-filtered grid-connected inverters using a reduced number of sensors," *IEEE Transactions on Industrial Electronics*, vol. 62, no. 10, pp. 5993-6002, Oct. 2015.
[13] J. Dannehl, F. W. Fuchs, S. Hansen *et al*., "Investigation of active damping approaches for PI-based current control of grid-connected pulse width modulation converters with LCL filters," *IEEE Transactions on Industry Applications*, vol. 46, no. 4, pp. 1509-1517, Jul. - Aug. 2010.
[14] A. Coccia, G. Escobar, L.-A. Serpa *et al*., "Control method for single-phase grid-connected LCL inverter," US Patent 8553434B2, Sept. 15, 2011.
[15] J. M. Sosa, P. R. Martinez-Rodriguez, G. Vazquez *et al*., "Model based controller for an LCL coupling filter for transformerless grid connected inverters in PV applications," in *Proceedings of 2013 39th Annual Conference of the IEEE Industrial Electronics Society (IECON)*, Vienna, Austria, Nov. 2013, pp. 1-6.
[16] S. G. Parker, B. P. McGrath, and D. G. Holmes, "Regions of active damping control for LCL filters," *IEEE Transactions on Industry Applications*, vol. 50, no. 1, pp. 424-432, Jan.-Feb. 2014.
[17] J. Xu, S. Xie, and T. Tang, "Active damping-based control for grid-connected LCL-filtered inverter with injected grid current feedback only," *IEEE Transactions on Industrial Electronics*, vol. 61, no. 9, pp. 4746-4758, Sept. 2014.
[18] M. Victor, F. Greizer, S. Bremicker *et al*., "Method of converting a direct current voltage from a source of direct current voltage, more specifically from a photovoltaic couse of direct current voltage, into an alternating current voltage," US Patent Application Publication US 2005/0286281 A1, Dec. 29, 2005.
[19] H. Schmidt, C. Siedle, and J. Ketterer, "DC/AC converter to convert direct electric voltage into alternating voltage or into alternating current," US Patent US 7046534 B2, Aug. 11, 2005.
[20] R. Gonzalez-Senosiain, J. Coloma-Calahorra, L. Marroyo-Palomo *et al*., "Single-phase inverter circuit for conditioning and converting DC electrical energy into AC electrical energy," WIPO (PCT) Patent WO 2008/015298 Al, Feb. 2008.
[21] T. Kerekes, R. Teodorescu, P. Rodriguez *et al*., "A new high-efficiency single-phase transformerless PV inverter topology," *IEEE Transactions on Industrial Electronics*, vol. 58, no. 1, pp. 184-191, Jan. 2011.
[22] A. Reznik, M. G. Simoes, A. Al-Durra *et al*., "LCL filter design and performance analysis for grid-interconnected systems," *IEEE Transactions on Industry Applications*, vol. 50, no. 2, pp. 1225-1232, Mar. - Apr. 2014.
[23] W. Wu, Y. He, and F. Blaabjerg, "An LLCL power filter for single-phase grid-tied inverter," *IEEE Transactions on Power Electronics*, vol. 27, no. 2, pp. 782-789, Feb. 2012.
[24] A. A. Valdez-Fernandez, P. R. Martinez-Rodriguez, G. Escobar *et al*., "A model-based controller for the cascade H-bridge multilevel converter used as a shunt active filter," *IEEE Transactions on Industrial Electronics*, vol. 60, no. 11, pp. 5019-5028, Nov. 2013.
[25] R. Teodorescu, F. Blaabjerg, M. Liserre *et al*., "Proportional-resonant controllers and filters for grid-connected voltage-source converters," *IEE Proceedings - Electric Power Applications*, vol. 153, no. 5, pp. 750-762, Sept. 2006.
[26] B. A. Francis, and W. M. Wonham, "The internal model principle for linear multivariable regulators," *Applied Mathematics and Optimization*, vol. 2, no. 2, pp. 170-194, Jun. 1975.
[27] V. Kaura and V. Blasko, "Operation of a phase locked loop system under distorted utility conditions," *IEEE Transactions on Industry Applications*, vol. 33, no. 1, pp. 58-63, Jan.-Feb. 1997.
[28] J. de Vegte, *Feedback Control Systems*, 3rd ed. Englewood Cliffs: Prentice Hall, 1993.
[29] P. R. Martinez-Rodriguez, J. M. Sosa, S. Iturriaga-Medina *et al*., "Model based current mode control design and experimental validation for a 3ϕ rectifier under unbalanced grid voltage conditions," *Journal of Modern Power Systems and Clean Energy*, vol. 6, no. 4, pp. 777-790, Jul. 2018.
[30] P. R. Martinez-Rodriguez, G. Escobar, A. A. Valdez-Fernandez *et al*., "Direct power control of a three-phase rectifier based on positive sequence detection," *IEEE Transactions on Industrial Electronics*, vol. 61, no. 8, pp. 4084-4092, Aug. 2014.
[31] P. Channegowda and V. John, "Filter optimization for grid interactive voltage source inverters," *IEEE Transactions on Industrial Electronics*, vol. 57, no. 12, pp. 4106-4114, Feb. 2010.
[32] M. Liserre, F. Blaabjerg, and S. Hansen, "Design and control of an LCL-filter-based three-phase active rectifier," *IEEE Transactions on Industry Applications*, vol. 41, no. 5, pp. 1281-1291, Sept.-Oct. 2005.

Jose M. Sosa received his Master and Ph. D. degrees in applied sciences from the Instituto Potosino de Investigacion Cientifica y Tecnologica (IPICYT), San Luis Potosi, Mexico, in 2009 and 2015, respectively. Since 2008, he has been holding a full-time Professor-Researcher position at Instituto Tecnologico Superior de Irapuato (TecNM / ITESI), Irapuato, Mexico. His research interests include control theory, analysis, design and control of power electronics converters and renewable energy systems.

Panfilo R. Martinez-Rodriguez received his Ph. D. degree in applied sciences from a Mexican Council of Science and Technology research center IPICyT, San Luis Potosi, Mexico, in 2007. From 2006 to 2017, he was a Professor-Researcher at the Technological Institute of Superior Studies of Irapuato (ITESI), Irapuato, Mexico. He is currently a professor at the School of Sciences at the Autonomous University of San Luis Potosi (UASLP), San Luis Potosi, Mexico. His contributions are mainly aimed on the fields of industrial electronics, power electronics and automatic control, where his main research interests include modeling, analysis, control design of power electronic systems for power quality and renewable energy systems.

Gerardo Escobar received his Ph. D. degree from the Signals and Systems Laboratory, LSS-SUPELEC, Université de Paris XI, Orsay, France. From 2008 to 2012, he was a Principal Scientist in the Power Electronics Group at ABB Switzerland Ltd. He is currently a Professor-Researcher in the School of Engineering and Sciences at Tecnologico de Monterrey, Nuevo Leon, Mexico. He is Senior Member of the IEEE since 2008. He is member of the National Research Fellows System level 3 (SNI-3), Consejo Nacional de Ciencia y Tecnología (CONACyT), Mexico. He served as Associate Editor (AE) of the IEEE Transactions on Industrial Electronics from 2007 to 2016. He is currently AE of the IEEE Transactions on Power Electronics since 2013. His main research interests include modeling, analysis, and control design of power electronic systems, and their applications in renewable energy systems, power quality, grid integration, active filters, inverters, DC-DC converters, multilevel converters, batteries, electrical drives, wind power, photovoltaic systems, as well as nonlinear control design, adaptive control, repetitive control, and their applications in current control, voltage balance, grid synchronization and harmonic compensation.

Gerardo Vazquez received the Ph. D. degree in electrical engineering from the Technical University of Catalonia, Barcelona, Spain, in 2013. In 2009, he was a Visiting Scholar at the Aalborg University, Aalborg, Denmark. He is member of the National Research Fellows System level 1 (SNI-1) of CONACyT, Mexico. Since 2012, he is with the Instituto Tecnologico Superior de Irapuato (TecNM / ITESI) holding a Full Time Professor-Researcher position at the Electronics Department. His research interests include the analysis and design of power electronics converters, renewable energy systems and grid connected converters.

Andres A. Valdez-Fernandez received the Ph. D. degree in control and dynamical systems from the Potosi Institute of Scientific and Technological Research (IPICyT), San Luis Potosi, Mexico, in 2009. From 2008 to 2012, he was a Professor-Researcher with the Technological Institute of Superior Studies of Irapuato (ITESI), Irapuato, Mexico. He is currently a professor with the Electronic Engineering Group of the School of Sciences, Autonomous University of San Luis Potosi (UASLP), San Luis Potosi, Mexico. His main research interests include analysis, modelling, fault diagnosis and con-

trol design of active power filters, inverters, rectifiers and renewable energy systems.

Juan F. Martinez-Garcia received the Master degree in electronics engineering from the Instituto Tecnologico Superior de Irapuato (ITESI), Irapuato, Mexico, in 2015. He is currently pursuing the Ph.D. degree in electronics engineering from the Universidad Autonoma de San Luis Potosi, San Luis Potosi, Mexico. His main research interests include power electronics converters applied to renewable energy systems.